Microporous and Mesoporous Materials 144 (2011) 183–190

Contents lists available at ScienceDirect

Microporous and Mesoporous Materials

journal homepage: www.elsevier.com/locate/micromeso

Synthesis, characterization and catalytic activity of AlSBA-3 mesoporous catalyst having variable silicon-to-aluminum ratios

María L. Martínez [a], Marcos B. Gómez Costa [a], Gustavo A. Monti [b], Oscar A. Anunziata [a,*]

[a] Grupo Fisicoquímica de Nuevos Materiales-CITeQ, Facultad Regional Córdoba, Universidad Tecnológica Nacional, 5016 Córdoba, Argentina
[b] Instituto de Física Enrique Gaviola, CONICET, Facultad de Matemática, Astronomía y Física, Universidad Nacional de Córdoba, 5016 Córdoba, Argentina

ARTICLE INFO

Article history:
Received 30 November 2010
Received in revised form 7 April 2011
Accepted 9 April 2011
Available online 14 April 2011

Keywords:
AlSBA-3
Strength acidity
Acid sites
Aluminum incorporation
Isopropanol dehydration

ABSTRACT

AlSBA-3 mesoporous catalytic materials with different Si/Al ratios were synthesized; Al was incorporated in the mesoporous structure using the post-synthesis method. The catalysts were characterized using different techniques and methods, such as: XRD, BET, ICP, SEM microcopy, TEM microscopy and ^{27}Al MAS NMR. Acidic properties were estimated by adsorption–desorption using pyridine as probe molecule followed by FTIR spectroscopy. FTIR studies showed the acidic properties with aluminum incorporation; lower Si/Al ratios increase the number of acid sites. Temperature-programmed desorption of pyridine showed that AlSBA-3 has a higher number of strong acid sites compared to other mesoporous materials such as Al-MCM-41, Al-SBA-15 and Al-SBA-16. It has been observed by ^{27}Al MAS NMR spectroscopy, that the materials exhibit peaks with shifts of 50 ± 2 ppm and weak signal at 0 ± 2 ppm. The AlSBA-3 materials used as a catalyst showed high performance in the acid-catalyzed dehydration of isopropanol.

1. Introduction

Since mesoporous molecular sieves (M41S) disclosure at the beginning of the 1990s [1], were intensively modified to confer catalytic properties. Isomorphic substitution of different hetero-atoms [2], principally aluminum, into M41S structure has been widely applied. However, the acidity of aluminum modified mesoporous materials was distinctively lower compared with i.e., zeolites [3,4].

In 1998, Zhao et al. [5,6]synthesized a new type of mesoporous materials, SBA-15 with uniform two-dimensional hexagonal. Compared with microporous zeolites, this material is characterized by larger pore sizes up to approximately 25 nm and allows bulky molecules to enter into the pores. Among different supports with ordered pore structure, SBA type materials seem to be more appropriate to be modified with aluminum than MCM-41, because they have larger pores, thicker pore walls and higher hydrothermal stability [7–10].

According with the results of Voegtlin et al. [11] and our earlier studies [12–14], balanced Coulombic, hydrogen bonding, and Van der Waals interactions with charge matching in aqueous synthesis, provide an effective means of enhancing long-range periodic order. Such interactions are particularly significant at the inorganic–organic interface and it can be obtained working with cationic silica species, below the aqueous isoelectric point of silica (pH ~ 2). The synthesis procedure with cationic surfactants, in HCl media below the aqueous isoelectric point of silica, the key interactions are among the cationic surfactant, chloride anion, and the cationic silica species; designated as $S^+X^-I^+$, where S^+ is the cationic surfactant, X^- is the halide anion, and I^+ is a protonated Si-OH moiety, and the overall charge balance is provided by association with an additional halide anion, [14,15].

SBA-type silica materials [16,17], are ordered mesoporous molecular sieves with higher hydrothermal stability than MCM-41 [18]. Moreover, the microporosity of SBA-3 was significantly larger than in SBA-15 [9,19–21]. SBA-3-type mesoporous molecular sieves were synthesized at room temperature (r.t.) under acid conditions [22] employing a similar procedure that SBA-15, except that different template were used for SBA-3, i.e., low-molecular-weight alkyl quaternary ammonium ions (CTA^+). Many investigations have indicated that Al-SBA-15 materials show much higher catalytic activity, compared with Al-MCM-41 [23,24]. Since pure siliceous SBA-15 materials lack acidity, active centers must be introduced into their framework (mesoporous wall). The incorporation of Al is particularly important as it gives rise to solid acid materials with acid sites associated with the presence of Al in framework positions, within the silica pore walls. Mesoporous aluminosilicates have therefore been the focus of many recent studies [25–27], because of their potential application in solid acid/base catalysis for bulky molecules activation. The traditional method of introducing Al into mesoporous silicates is the direct (mixed-gel) synthesis where, an aluminosilicate framework is formed directly from aluminate and silicate ions. Generally, the heteroatom incorporation, such as Al into microporous zeolites

* Corresponding author. Tel./fax: +54 351 4690585.
E-mail address: oanunziata@scdt.frc.utn.edu.ar (O.A. Anunziata).

1387-1811/$ - see front matter © 2011 Elsevier Inc. All rights reserved.
doi:10.1016/j.micromeso.2011.04.010

will introduce a charge imbalance in the framework, which is counterbalanced by protons, generating bridging hydroxyl groups (SiO_3–O_3–Al–OH, Brønsted acid sites) on these materials.

However, it is very difficult to introduce the metal ions directly into SBA's due to the easy dissociation of metal-O–Si bonds under strong acidic conditions. Thus, the post-synthesis method for the alumination of the mesoporous silicas, which are obtained under strongly acid conditions, becomes an appealing alternative [28]. Many studies have shown that aluminum can be effectively incorporated into siliceous MCM-41 and MCM-48 materials, via various post-synthesis procedures. The authors claimed that the materials produced via the post-synthesis method have superior structural integrity, acidity, and catalytic activity than those of materials having aluminum incorporated during synthesis [29–32]. Recently Anunziata et al. [33] have published a synthesis of Na–Al–SBA-3 with high-framework aluminum contents, without any significant loss in textural properties of SBA-3, by the treatment of pure silica SBA-3 with an aqueous solution of $NaAlO_2$ at room temperature. Gómez-Cazalilla et al. [34] and Lin et al. [35] have examined the acidity of Al-SBA-15 materials. Luan et al. [36] studied synthesis of AlSBA-15 with different aluminum source.

Here we present the synthesis, characterization and the evaluation of the acid properties of a series of AlSBA-3 materials with different aluminum content obtained by post-synthesis alumination [33]. The preparation of the mesoporous silica was based on the procedure proposed by Anunziata et al. [33]. The materials were fully characterized by different physicochemical methods showing a high-framework aluminum content (up to a bulk Si/Al ratio of 10) and good structural integrity. The nature of acid sites in AlSBA-3 has been studied using pyridine as probe molecule and by catalytic tests of 2-propanol dehydration.

2. Experimental

2.1. Synthesis

The mesoporous aluminosilicate was synthesized by hydrolysis of tetraethylorthosilicate (TEOS) at room temperature, in an aqueous acidic solution, using cetyltrimethylammonium bromide (CTAB) as surfactant. The designed procedure was the following: the surfactant was mixed with water and HCl; then, 3 g of TEOS were added, stirring to form a mixture with a molar composition of: TEOS:H_2O:HCl:CTAB = 1:130:9.2:0.12 [33]. After 45 min, a white precipitate was obtained, and then it was filtered, washed and dried at room temperature. The material was then, immersed in ethanol reflux for 6 h in order to extract the surfactant and calcined at 823 K in air for 6 h. The obtained material was denoted as SBA-3. The alumination procedure of SBA-3 was carried out as follows [26,35]: Silica SBA-3 (1 g) was stirred in 50 ml of water, containing dissolved sodium-aluminate in different proportions, at room temperature for 20 h and pH of 5.6. The synthesis was carried out at this pH, because sodium aluminate is not stable in acid medium (pH < 3), and it reacts rapidly with protons to generate aqueous Al^{3+} ions; if pH is higher, deposition of aluminum hydroxide will occur. The mixture was filtered, washed, dried at room temperature overnight and then calcined in air at 823 K for 5 h. Finally, Al-SBA-3 sample with different Si/Al ratios were obtained.

2.2. Preparation of H-AlSBA-3

Calcined Na-AlSBA-3 mesoporous material was put into 1 M NH_4Cl solution, and stirred at 353 K for 20 h. The ion exchange was repeated two times [33]. The solid was filtered, washed with deionized water and dried at 383 K for 2 h. The solid powder was then calcined at 723 K for 5 h. The solid powders of H-AlSBA-3 with Si/Al ratio of 10, 15, 20 and 30 were denoted as H-10, H-15, H-20 and H-30, respectively.

2.3. Catalytic activity

The catalytic decomposition of 2-propanol (isopropanol) was used as a test reaction for the study of the effective acidity. A fixed bed tubular glass reactor (20 cm long and 0.5 cm i.d.) working at atmospheric pressure was used. The catalyst (H-AlSBA-3) was diluted in crushed quartz (50 mg catalyst/700 mg quartz).

The 2-propanol (Sintorgan, 99%) was fed into the reactor (0.5 mol/h) by a continuous-flow apparatus (positive displacement pump) at atmospheric pressure and flowing N_2 at 25 ml/min, which gave a constant isopropanol flow [21]. The reaction products were analyzed by an on-line gas chromatograph (HP 5890) provided with a FID detector and a capillary column Supelco Petrocol DH 100 m × 0.25 mm i.d. The conversion and selectivity were defined as mole percentage.

2.4. Method and characterization

FTIR spectra for acidic properties of the samples were obtained with self-supported wafers in a vacuum cell with CaF_2 windows in a JASCO 5300 Fourier Transform Spectrometer. The nature (Brønsted and Lewis sites) and acid strength of the samples were determined by pyridine (Py) adsorption/desorption. The samples were desorbed at 673 K during 4 h ($p < 10^{-1}$ Pa). Py (667 Pa) was adsorbed at room temperature overnight. Then, it was desorbed for 1 h in vacuum (2.6 Pa) at room temperature, 373, 473, 573 and 673 K. On the other hand, the fingerprints of the samples were obtained using wafers of SBA in KBr in a vacuum cell with KBr windows. XRD patterns were recorded in the Philips X'Pert PRO PANalytical diffractometer under Cu Kα radiation ($\lambda = 1.5418$). Solid state NMR spectra were taken on a BRUKER AVANCE II 300 spectrometer operating at 78.2 MHz for ^{27}Al. We used a BRUKER MAS 300WB CP1H-BBWH. VTN-BL4 probe with 4 mm o.d. zirconia rotors with the following experimental conditions: single pulse acquisition with proton decoupling and rotation, at the magic angle (MAS), with an excitation pulse of $\pi/10 = 1.0$ μs, MAS speed 10 kHz, number of acquisitions 12288, recycle delay 1 s.

Elemental analysis was performed by inductively coupled plasma-atomic emission spectroscopy (VISTA-MPX), operated with high frequency emission power of 1.5 kW and plasma airflow of 12.0 L/min. The surface area was determined by the BET method using a MICROMERITICS Chemisorb 2720 apparatus, equipped with a TCD detector. Scanning electron micrographs (SEM) were obtained by using a Nova NANOSEM 230 with EDS (FEI COMPANY). Samples were placed over an aluminum drum and covered with a gold film. The transmission electron microscopy (TEM) micrographs were taken on a TEM Philips EM 301 instrument, operated at 100 kV.

3. Results and discussion

3.1. XRD analysis

The X-ray diffraction patterns of as made SBA-3 and AlSBA-3 materials are illustrated in Fig. 1a and b, respectively, showing the reflection peaks in the low angle region, characteristic of mesostructures. The presence of three Bragg angles can be distinguished in hexagonal lattice symmetry, typical of SBA-3 structure. Moreover, XRD patterns indicate that the hexagonally ordered structure of SBA-3 was persistent after the modification procedure. A prominent peak, hkl = [1 0 0] as well as weaker peaks of [1 1 0] and [2 0 0] were observed in XRD pattern of SBA-3, which

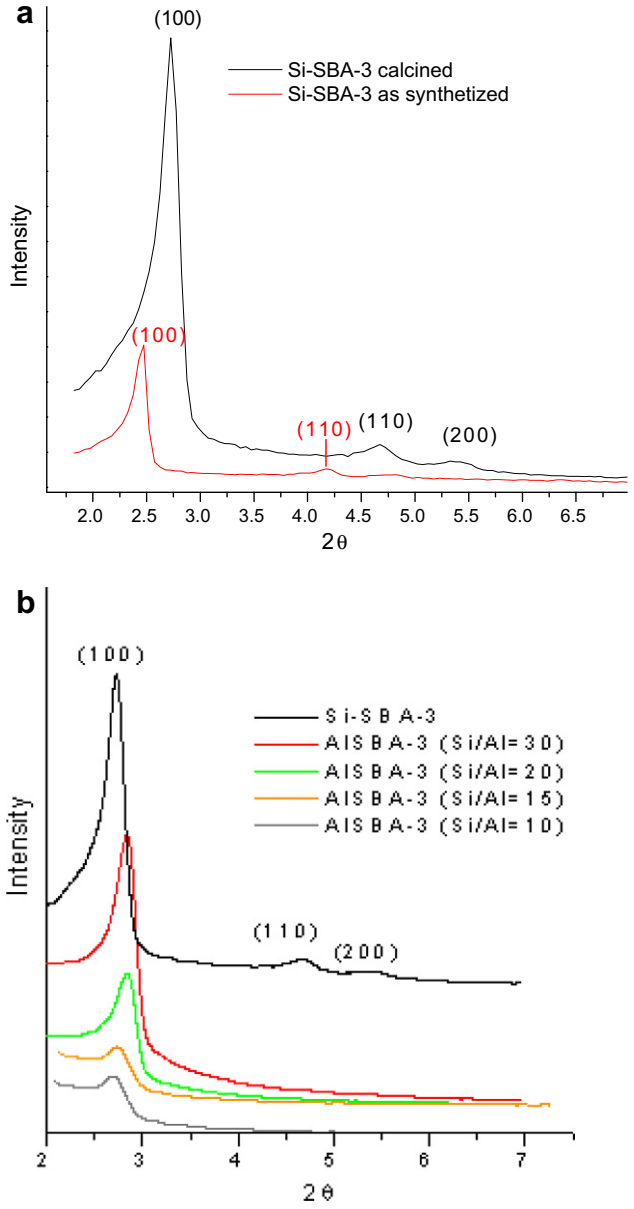

Fig. 1. (a) XRD of SBA-3 as synthesized and calcined and (b) XRD of AlSBA-3 with different Si/Al ratios.

allowed us to corroborate, that the obtained mesoporous sample has a highly ordered pore system with a high porosity. XRD parameters were shown in Table 1.

The XRD pattern for the as-synthesized sample exhibits a strong [1 0 0] reflection peak with two small peaks, characteristics of SBA-3 material. After the template was removed by calcination, the intensity of [1 0 0] diffraction was slightly increased, this indicates that proper calcinations lead to a better-defined structure of SBA-3.

Fig. 1b shows that diffraction patterns of aluminated samples suggest the preservation of the SBA-3 structure after incorporation of Al by post-synthesis methods.

Only a slight broadening of the (1 0 0) reflection peaks for the AlSBA-3 obtained by post-synthesis can be observed, as well as a slight shifting of the (1 0 0) peak to higher 2θ values and lower d-spacing after Al incorporation (Table 1). The same behavior has been reported for Al-SBA-15 obtained by grafting [37]. This behavior might possibly be caused by a slight distortion of the mesoporous channels due to the partial polymerization over pore structures induced by superficial reaction (see Fig. 2).

Table 1
Structural properties of samples.

Sample	Si/Al		XRD		A_{BET} (m^2/g)
	Gel	ICP	d_{100}* (nm)	a_0* (nm)	
SBA-3	∞	∞	3.13	3.6	1024
H-30	30	29.8	3.10	3.6	810
H-20	20	20.2	2.95	3.4	770
H-15	15	15.4	2.91	3.4	620
H-10	10	10.2	2.82	3.2	580

* d[hkl]: interplanar spacing; a_0: lattice parameter ($a_0 = 2d[100]/\sqrt{3}$).

3.2. BET studies

The BET specific surface area decreases with the Al content, from 1024 (pristine SBA-3) to 580 m^2/g for AlSBA-3 Si/Al = 10, due to the occupation of guest species on the surface of the pores as well as the in equable contribution of the additional mass Al_2O_3 in the sample. This trend is in good agreement with the results of Ooi et al. [38], who found that too high an aluminum loading stimulates the deterioration of pore structure. However, the reduction in the surface area of the AlSBA-3 samples, compared with pure silica SBA-3, might be due to the partial polymerization over pore structures induced by superficial reaction (see Fig. 2).

3.3. ICP results

The chemical analysis of AlSBA-3 materials synthesized using sodium aluminate as the Al source with different Si/Al ratio is summarized in Table 1. The Si/Al ratios of the Al-SBA-3 materials are in good agreement with the composition in the post-synthesis alumination mixtures (10, 15, 20 and 30). This suggest that aluminum atoms have been successfully incorporated to the pore surface of mesoporous SBA-3 structure by this post-alumination procedure, see Table 1 and the proposed model of Al incorporation, Fig. 2 .

3.4. TEM and SEM microscopy

An ordered channels array could be observed from the TEM micrograph for SBA-3 sample (Fig. 3a), therefore mesoporous silica particle exhibits a well-ordered mesostructure a typical honeycomb structure (cylindrical pores are viewed from the side as a stripped image).

To establish the morphology of the aluminated materials, the SEM studies reveal that the incorporation of aluminum in the pores of SBA-3 has no apparent effects on the macroscopic morphology of the samples (Fig. 3b). The SEM images of the samples show aggregates of regular spherulitic-shaped particles for Si/Al = 20 ratio. The particle size of the AlSBA-3 was approximately 2–4 μm in diameter. The well-regular shape is the same in all of aluminated materials.

3.5. Skeletal FTIR studies

The IR lattice vibration spectra in the 600–1300 cm^1 region of calcined samples show the bands resulting from a typical siliceous material, with a main band at 1080 cm^1 and a shoulder at 1227 cm^1, due to asymmetric Si–O–Si stretching modes. There is also a weaker band at 800 cm^1, due to Si–O–Si symmetric stretching modes (Fig. 4). It is noteworthy that the incorporation of aluminum causes a decrease or disappears in intensity of the component assigned to the Si-(OH) stretching mode at 960 cm^{-1}. This result is

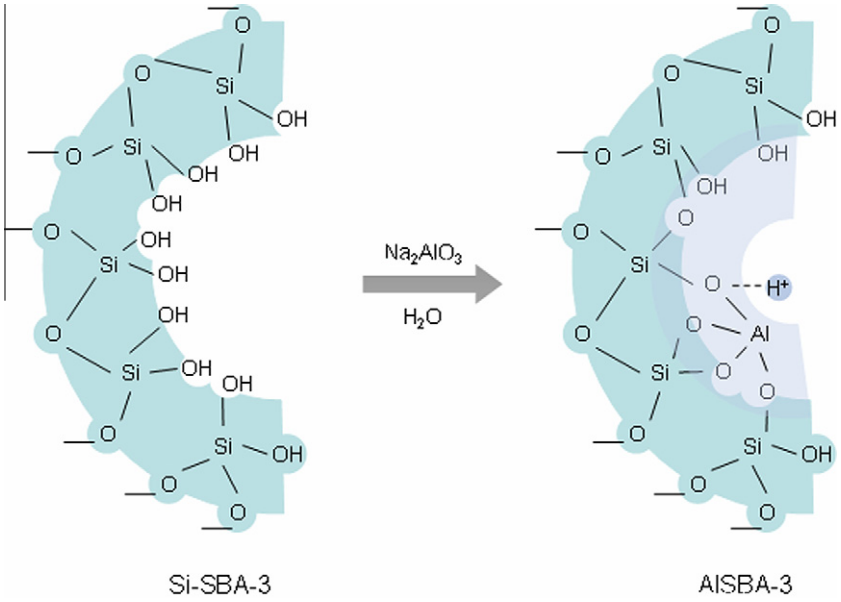

Fig. 2. Possible structure of AlSBA-3.

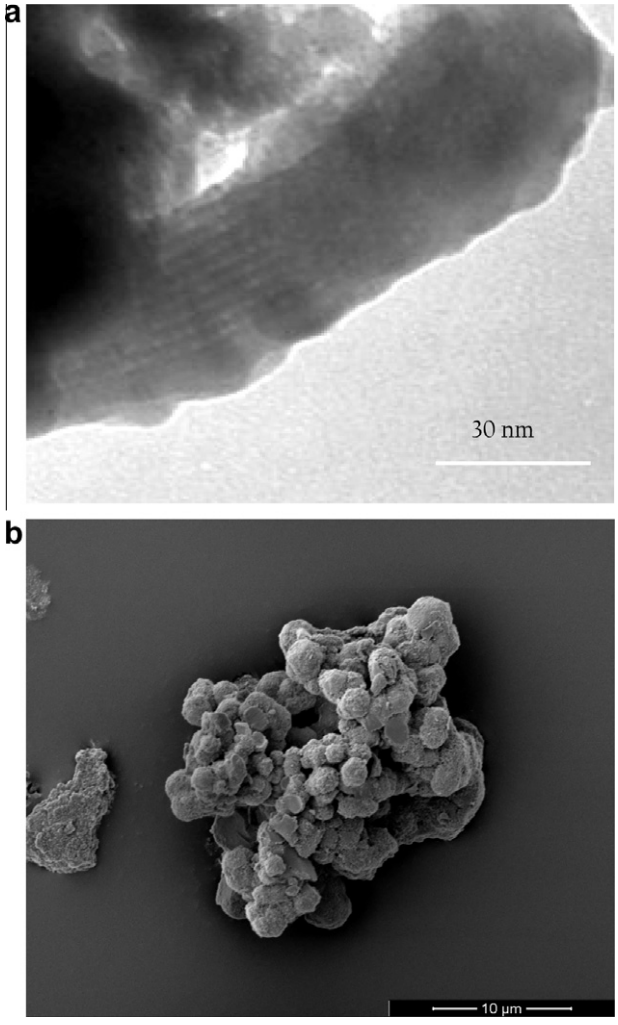

Fig. 3. (a) TEM micrograph of SBA-3 material and (b) SEM micrographs of AlSBA-3 Si/Al = 20 catalytic materials.

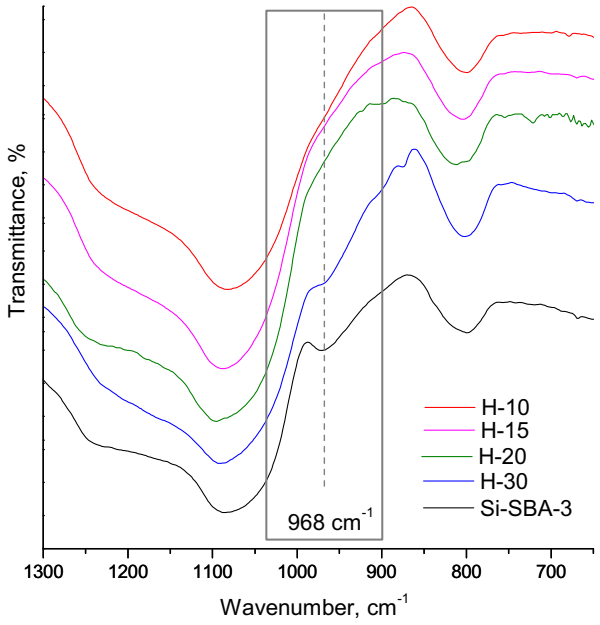

Fig. 4. FTIR finger print of Si-SBA-3 and AlSBA-3 catalysts with different Si/Al ratios.

understandable with the post-synthesis incorporation of aluminum, since it is introduced into the mesoporous walls via a condensation process of the oxo-hydroxo species of aluminum with the silicon species, such as the Si-(OH) terminal groups.

3.5.1. ^{27}Al MAS NMR spectroscopy

Fig. 5 shows ^{27}Al solid-state MAS-NMR spectra of the AlSBA-3 samples with different Si/Al ratios.

The spectra exhibit peaks with chemical shifts of 50 ± 2 ppm and very low intensity signals at 0 ± 2 ppm.

The resonance at 50 ± 2 ppm is assigned to tetrahedral coordinated framework aluminum (Td–Al) and resonance at 0 ± 2 ppm is assigned to octahedral coordinated (OH–Al) non-framework aluminum [33,39]. As it can be observed, aluminum was incorporated mainly with tetrahedral coordination in the framework of SBA-3

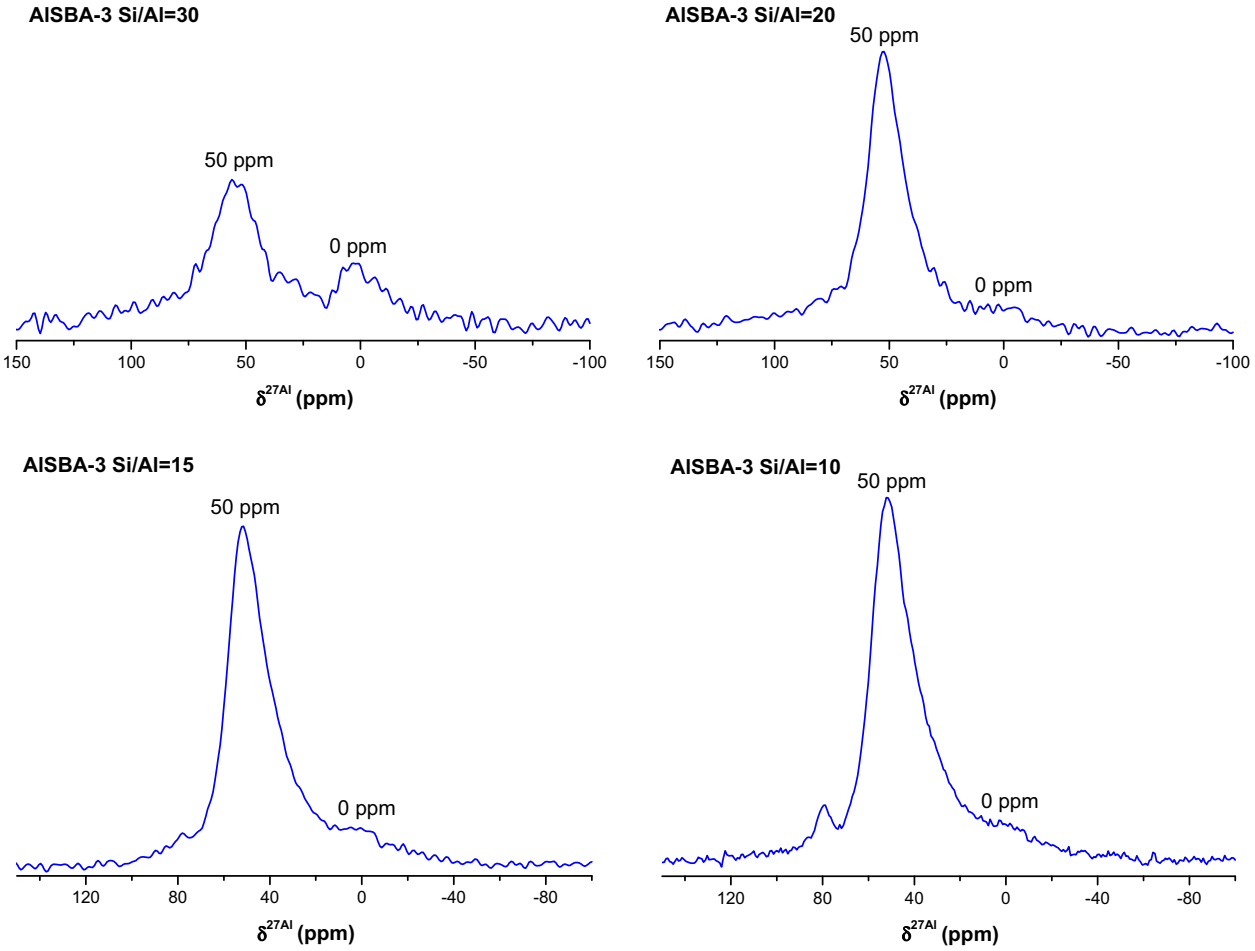

Fig. 5. AS-NMR ^{27}Al solid-state MAS-NMR spectra of the AlSBA-3 samples with different Si/Al ratios.

samples prepared by the post-synthesis procedure, mainly in samples with Si/Al = 15 and Si/Al = 10, that exhibits a strong resonance at 50 ± 2 ppm indicating that almost a greater proportion of incorporated aluminum atoms are in tetrahedral coordination.

3.6. Acidic surface properties

Pyridine (Py) adsorption on acid catalysts has been used to characterize the nature, number and strength of acid sites through infrared analysis. Thus, we determined the acid strength of the sites, based on the capacity to retain Py adsorbed in anchor sites increasing the desorption temperature. Pyridine is a weak basic molecule, hence it can only titrate stronger acid sites. However, it is able to neutralize both Brønsted and Lewis acid sites. Fig. 6 shows the infrared spectra of Py adsorbed at room temperature, and desorbed in vacuum at different temperatures for samples SBA-3, H-10, H-15, H-20 and H-30. The different curves represent the evolution of the retained Py as temperature increases. The bands observed at 1444, 1454, 1491, 1547, 1579, 1597, 1624 and 1641 cm^{-1} are due to the chemisorption of Pyridine.

According to the literature data [34,40] the siliceous material, after evacuation at room temperature, presents the bands at 1597 and 1444 cm^{-1} that are assigned to hydrogen-bonded pyridine (PyH^+).

In Al-containing SBA-3 samples the bands at 1454 and 1624 cm^{-1} are due to strong pyridine bound to Lewis sites; the band at 1579 cm^{-1} is due to weak Lewis-bound pyridine and the bands at 1547 and 1641 cm^{-1} to pyridinium ion ring vibration due to pyridine bound to Brønsted acid sites. A band at 1491 cm^{-1} was assigned to pyridine associated with both, Brønsted and Lewis sites [40–42]. A quantitative evaluation of acid sites, both Brønsted and Lewis, for samples under different desorption temperatures (373, 473, 573 and 673 K), are shown in Table 2. The integrated molar extinction coefficients used take the following values: 1.67 cm/μmol for Brønsted acid sites and 2.22 cm/μmol for the Lewis acid site [43]. To make an approach, we assumed that these coefficients and their ratio remain constant in the temperature range studied.

The hydrogen-bonded pyridine bands decrease faster when the samples are outgassed at low temperatures. However, the strength of the acid sites is strong because its bands decrease slowly when desorption takes place (373, 473, 573 and 673 K) and still exists pyridine adsorbed onto Lewis and Brønsted acid sites when samples desorbed at 673 K (see Fig. 6).

The presence of a significant amount of pyridine molecules adsorbed at 473 K (see Table 2) compared with others mesoporous materials [40,44] indicates a great presence of acid sites at least with moderate strength. We can assume that the incorporation of Al gives rise to a greater amount of moderate-strong Brønsted acid sites in the form of Si–O(H)–Al bridges.

Table 2 shows generally that number of Brønsted acid sites increase while Si/Al ratio decrease and shows that the proportion of extra-framework Al species generally decrease with the increase in the amount of aluminum in samples. Pyridinium ions (PyH^+) on Brønsted sites also decrease with heat treatment. However, this reduction appears to be relatively lower than Lewis acid sites at

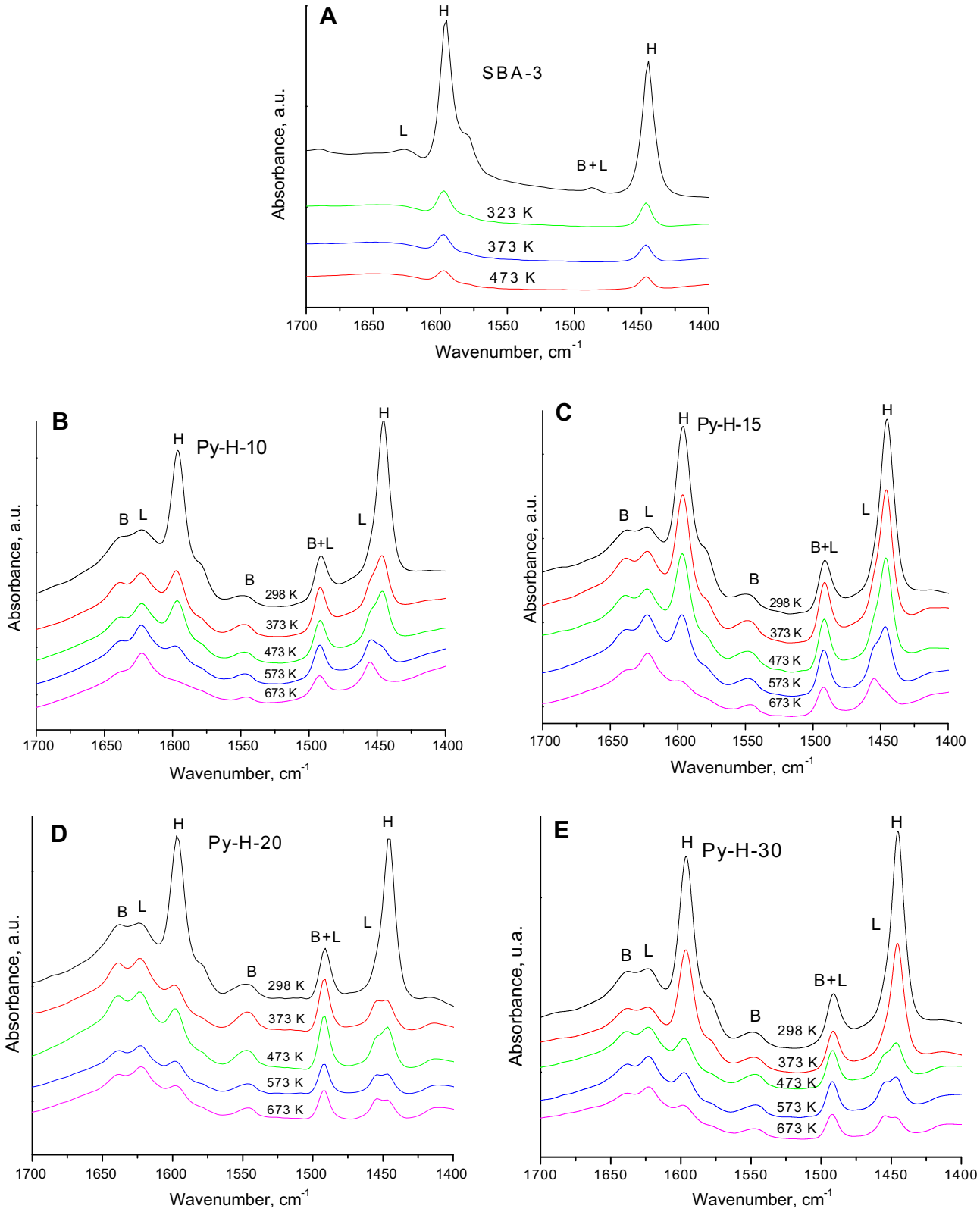

Fig. 6. Pyridine desorption FTIR spectra of (A) SBA-3 and (B) H-10, (C) H-15, (D) H-20 and (E) H-30 at different desorption temperatures: room temperature, 373, 473, 573 and 673 K.

373 K, increasing the ratio of Brønsted acid sites compared to Lewis at higher desorption temperatures. Klimova et al. [40], have studied the acid properties of Al-SBA-15 (Si/Al = 20) at 373 K. They have obtained a sample with 61 μmol Py/gr, whereas in this work we have obtained a much higher amount of Py retained at the same conditions, indicating a greater density and stronger acidity of the synthesized AlSBA-3 in comparison with others Al-SBA conventionally prepared [10,11,33].

The nature of surface hydroxyls was evaluated by FTIR spectroscopy after thermal treatment at 673 K (Fig. 7). The stretching of Si-

Table 2
Total number of Brønsted and Lewis sites in AlSBA-3 with different Si/Al ratios.

AlSBA-3 Temp. K	Brønsted (μmol Py/g)*				Brønsted (μmol Py/g)*				Brønsted/Lewis	
	373	473	573	673	373	473	573	673	373	573
H-30	108	56	55	36	41	33	28	21	2,62	1,97
H-20	127	126	119	84	53	48	43	41	2,40	2,75
H-15	137	127	123	70	84	68	65	31	1,64	1,89
H-10	277	255	214	162	297	137	129	129	0,93	1,65

* Curve fitting calculations in FTIR spectra (Fig. 6) were useful for determining bands areas. The fitting confidence was $\chi^2 = 1\ 10^{-5}$ and $R^2 = 0.99$. The amount of Py adsorbed on Brønsted (B) and Lewis (L) sites per gram of catalyst, is obtained by using the following equation: C (pyridine on B sites) = 1.88 IA (B) R^2/W; C (pyridine on L sites) = 1.42 IA (L) R^2/W, where C = concentration (mmol/g catalyst), IA (B and L) = integrated absorbance bands of B or L(cm^{-1}), R = radius of catalyst wafer (cm), W = weight of the wafer (mg) [43].

OH band (3742 cm^{-1}), decreases in the intensity when Al is incorporated, confirming the grafting of Al on the surface silanol groups. The intensity of this band continues to decrease significantly with the Al content. However, even for the sample with Si/Al = 10, the Si-OH band is still visible. Whatever, Al-OH bands were scarcely observable (a very weak and broad shoulder between 3710 and 3725 cm^{-1} centered at 3715 cm^{-1}, may reveal the presence of these groups [45,46]), probably due to the low extinction coefficient of these vibrations. No band characteristic of Si–O(H)–Al group is observed in agreement with previously published work on alumino-silicates [47].

3.7. Isopropanol dehydration

Isopropanol conversion is often applied as catalytic tests to obtain the effective catalytic properties of acid centers. Thus, in the isopropanol conversion, catalysts can be classified according to their degree of acidity in dehydration or the dehydrogenation of propene or acetone, respectively. Thus, dehydration of isopropanol to propylene takes place on acid sites, whereas dehydrogenation to acetone is accomplished on redox or basic sites [34].

The conversions obtained at different temperatures are compiled in Table 3. While in this reaction, Si-SBA-3 is not active (at 473 K, <0.2% conversion), the catalysts containing aluminum exhibit a high conversion at 473 K, but it is very low at 423 K. The conversion is higher for the catalyst with higher Al content.

For higher Al contents an increase in the conversion takes place, indicating that the dispersion of aluminum species on the inner wall of the pores was satisfactory and thus, the number of aluminum acting as acid sites became increased. This fact is in good agreement with the results obtained from ^{27}Al MAS-NMR and Py desorption analyses. The selectivity was >75% at 473 K for propene for all the Si/Al ratios.

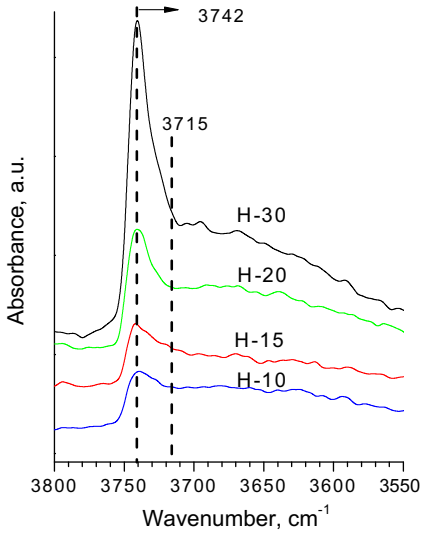

Fig. 7. nfrared spectra for H-AlSBA-3 catalysts for different Si/Al content at 673 K to 3800 cm^{-1} from 3550 cm^{-1}.

Table 3
Conversion (%) of 2-propanol and selectivity (%) to propylene at two different reaction temperatures, in the steady state, over different Al-SBA-3 samples.

	Si/Al = 30		Si/Al = 20		Si/Al = 15		Si/Al = 10	
	Conv.	Select.	Conv.	Select.	Conv.	Select.	Conv.	Select.
423 K	4.24	78.20	4.57	65.89	7.52	66.01	13.60	90.50
473 K	38.87	90.88	53.83	76.32	54.98	83.25	56.03	96.30

W/F = 0.1 g h mol^{-1}.

4. Conclusions

This work provides an efficient route for synthesizing new Al-SBA-3 catalysts with high-framework Al content, prepared by treating silica SBA-3, obtained from TEOS and CTAB aqueous solutions, with sodium aluminate by an post-alumination procedure. The samples were fully characterized by different physicochemical methods showing a high-framework aluminum content (up to a bulk Si/Al ratio of 10) and good structural integrity. ^{27}Al MAS-NMR studies have confirmed that this post-synthesis method is a good route to incorporate aluminum to a mesoporous silica SBA-3 in tetrahedral coordination. Pyridine adsorption results show that this series of catalytic materials has both Lewis and Brønsted acid sites. Moreover, the density of acid sites depends on the amount of aluminum incorporated into the siliceous framework, although the samples with the highest Al contents show better catalytic activity in selective dehydration of 2-propanol to propene. This fact could be explained due to the great dispersion of aluminum species on the inner wall of the pores in the Al-SBA-3 with high Al contents.

Acknowledgments

MBGC, GAM and OAA CONICET Researchers; MLM CONICET postdoctoral fellowship, are grateful to CONICET, Argentina, PIP N 112-200801-00388 (2009–2011) and PIP No. 112-2009-0100754 (2010–2012) and MinCyT-CBA PID: 1210/07 – (2007–2011).

References

[1] J.S. Beck, J.C. Vartuli, W.J. Roth, M.E. Leonowicz, C.T. Kresge, K.D. Schmitt, C.T.-W. Chu, D.H. Olson, E.W. Sheppard, S.B. McCullen, J.B. Higgins, J.L. Schlenker, J. Am. Chem. Soc. 114 (1992) 10834–10843.
[2] R. Ryoo, Sh. Jun, J.M. Kim, M.J. Kim, Chem. Commun. (1997) 2225–2226.
[3] A. Corma, Chem. Rev. 97 (1997) 2373–2420.

[4] A. Corma, V. Fornés, M.T. Navarro, J.J. Pérez-Pariente, J. Catal. 148 (1994) 569–574.
[5] D. Zhao, J. Feng, Q. Huo, N. Melosh, G.H. Fredrckson, B.F. Chmelka, G.D. Stucky, Science 279 (1998) 548–552.
[6] D. Zhao, Q. Huo, J. Feng, B.F. Chmelka, G.D. Stucky, J. Am. Chem. Soc. 120 (1998) 6024–6036.
[7] T. Yamada, H. Zhou, K. Asai, I. Honma, Mater. Lett. 56 (2002) 93–96.
[8] M. Mesa, L. Sierra, J.-L. Guth, Micropor. Mesopor. Mater. 112 (2008) 338–350.
[9] Z. Jin, X. Wang, X. Cui, Colloids Surf. A 316 (2008) 27–36.
[10] P. Wu, T. Tatsumi, Chem. Mater. 14 (2002) 1657–1664.
[11] A.C. Voegtlin, F. Ruch, J.L. Guth, J. Patarin, L. Huve, Microporous Mater. 9 (1997) 95–105.
[12] A. Firouzi, D. Kumar, L.M. Bull, T. Besier, P. Sieger, Q. Huo, S.A. Walker, J.A. Zasadzinski, C. Glinka, J. Nicol, D. Margolese, G.D. Stucky, B.F. Chmelka, Science 267 (1995) 1138–1143.
[13] A. Firouzi, F. Atef, A.G. Oertli, G.D. Stucky, B.F. Chmelka, J. Am. Chem. Soc. 119 (1997) 3596–3610.
[14] Q. Huo, D.I. Margolese, G.D. Stucky, Chem. Mater. 8 (1996) 1147–1160.
[15] Q. Huo, D.I. Margolese, P. Ciesia, Feng, T.E. Gier, P. Sieger, R. Leon, P.M. Petroff, F. Schüth, G.D. Stucky, Nature 368 (1994) 317–318.
[16] Q. Huo, D.I. Margolese, U. Ciesla, D.G. Demuth, P. Feng, T.E. Gier, P. Sieger, A. Firouzi, B.F. Chmelka, F. Schüth, G.D. Stucky, Chem. Mater. 6 (1994) 1176–1191.
[17] D. Zhao, J. Feng, Q. Huo, N. Melosh, G.H. Frederickson, B.F. Chmelka, G.D. Stucky, Science 279 (1998) 548–552.
[18] F. Kleitz, W. Schmidt, F. Schüth, Micropor. Mesopor. Mater. 65 (2003) 1–29.
[19] P.A. Albouy, A. Ayral, Chem. Mater. 14 (2002) 3391–3397.
[20] R. Ryoo, C.H. Ko, M. Kruk, V. Antochshuk, M. Jaroniec, J. Phys, Chem. B 104 (2000) 11465–11471.
[21] F. Chen, Xu. X-J, S. Shen, S. Kawi, K. Hidajat, Microporous Mesoporous Mater. 75 (2004) 231–235.
[22] O. Anunziata, A. Beltramone, L. Martínez, L. López Belon, J. Coll, Interf. Sci. 315 (2007) 184–190.
[23] A. Vinu, B.M. Devassy, S.B. Halligudi, W. Bohlmann, M. Hartmann, Appl. Catal. A: Gen. 281 (2005) 207–213.
[24] A. Vinu, D.P. Sawant, K. Ariga, M. Hartmann, S.B. Halligudi, Micropor. Mesopor. Mater. 80 (2005) 195–203.
[25] G.A. Eimer, M.B. Gómez Costa, L.B. Pierella, O.A. Anunziata, J. Coll, Interf. Sci. 263 (2003) 400–407.
[26] W. Hu, Q. Luo, Y. Su, L. Chen, Y. Yue, C. Ye, F. Deng, Micropor. Mesopor. Mater. 92 (2006) 22–30.
[27] J.M.R. Gallo, C. Bisio, L. Marchese, H.O. Pastore, Micropor. Mesopor. Mater. 111 (2008) 632–635.
[28] H.M. Kao, C.C. Ting, S.W. Chao, J. Mol. Catal. A: Chem. 235 (2005) 200–205.
[29] M. Xu, W. Wang, M. Seiler, A. Buchholz, M. Hunger, J. Phys. Chem. B 106 (2002) 3202–3208.
[30] Q. Xia, K. Hidajat, S. Kawi, J. Catal. 205 (2002) 318–331.
[31] J.M. Campelo, D. Luna, R. Luque, J.M. Marinas, A.A. Romero, J.J. Calvino, M.P. Rodríguez-Luque, J. Catal. 230 (2005) 327–338.
[32] R. Luque, J.M. Campelo, D. Luna, J.M. Marinas, A.A. Romero, Micropor. Mesopor. Mater. 84 (2005) 11–20.
[33] O.A. Anunziata, M.L. Martínez, M. Gomez, Costa. Mater. Lett. 64 (2010) 545–548.
[34] M. Gómez-Cazalilla, J.M. Mérida-Robles, A. Gurbani, E. Rodríguez-Castellón, A. Jiménez-López, J. Solid. State Chem. 180 (2007) 1130–1140.
[35] N. Lin, J.Y. Yang, Z.Y. Wu, H.J. Wang, J.H. Zhu, Micropor. Mesopor. Mater. 139 (2011) 130–137.
[36] Z. Luan, M. Hartmann, D. Zhao, W. Zhou, L. Kevan, Chem. Mater. 11 (1999) 1621–1627.
[37] B. Dragoi, E. Dumitriu, C. Guimon, A. Auroux, Micropor. Mesopor. Mater. 121 (2009) 7–17.
[38] Y. Ooi, R. Zakaria, A. Rahman Mohamed, S. Bhatia, Catal. Commun. 5 (2004) 441–445.
[39] O. Anunziata, A. Beltramone, J. Cussa, Catal. Today 133–135 (2008) 891–896.
[40] T. Klimova, J. Reyes, O. Gutiérrez, L. Lizama, Appl. Catal. A: Gen. 335 (2008) 159–171.
[41] T. Kataoka, J. Dumesic, J. Catal. 112 (1988) 66–79.
[42] B. Chakraborty, B. Viswanathan, Catal. Today 49 (1999) 253–260.
[43] C. Emeis, J. Catal. 141 (1993) 347–354.
[44] M. Boutros, T. Onfroy, P. Da Costa, Catal. Lett. 139 (2010) 50–55.
[45] H. Knozinger, P. Ratnasamy, Catal. Rev. Sci. Eng. 17 (1978) 31.
[46] M. Digne, P. Sautet, P. Raybaud, P. Euzen, H. Toulhoat, J. Catal. 211 (2002) 1.
[47] M. Baca, E. de la Rochefoucauld, E. Ambroise, J.-M. Krafft, R. Hajjar, P.P. Man, X. Carrier, J. Blanchard, Microp. Mesop. Mat. 110 (2008) 232.